Proceedings of the 3rd IASME/WSEAS Int. Conf. on FLUID DYNAMICS & AERODYNAMICS, Corfu, Greece, August 20-22, 2005 (pp224-229)

Numerical Study of Separating and Reattaching Flow over a Rectangular Wall-mounted Obstacle

PSYCHOUDAKI S.P., FRAGOS V.P.
Department of Hydraulics, Soil Sciences and Agricultural Engineering
Aristotle University of Thessaloniki
541 24 Thessaloniki
GREECE
papoutsi@agro.auth.gr
http://www.auth.gr/agro/eb/hydraul/intex.htm
MALAMATARIS N.A.
Department of Mechanical Engineering
Technological and Educational Institute of West Macedonia
501 00 Kila, Kozani
GREECE
nikolaos@eng.auth.gr

Abstract: - A numerical study of a flow over a rectangular wall-mounted obstacle has been investigated, using a DNS turbulent model. The two-dimensional Navier-Stokes and the continuity equations are solved using the finite element method. Turbulent flow characteristics of the flow are presented and compared numerically and qualitatively with other works. Instantaneous and time mean-averaged profiles of the velocity components and time mean-averaged distribution of the wall shear stress are presented. The fluctuations of velocity components and the energy spectrum analysis are given. The skin friction coefficient and the turbulent intensities are also presented.

Key-Words: Simulation of Navier-Stokes equations, finite element method, turbulent flow, separation and reattachment.

1. Introduction

The effects of a separation and reattachment flow has been studied by many investigators, experimentally and numerically [1, 2, 3, 4, 5, 7, 8, 9, 11 and many others]. Many numerical investigations are based on a κ-ε model [2,7], others on Large Eddy Simulation (LES) [1] and some on Direct Numerical Simulation (DNS) [5,6,9]. In the present work the flow over a mounted-obstacle is studied numerically, using the Direct Numerical Simulation (DNS) for a 2D turbulent flow. The model can calculate small and large vortices because of the small size of time step Δt and grid spacing Δx and Δy. The numerical method used was the finite elements, Galerkin method.

2. Covering Equations

The flow has been simulated in a wind tunnel and is nominated to be 2D, turbulent flow over a rectangular mounted-obstacle. The fluid is incompressible, Newtonian. There is also no gravity or other external power influences upon the flow. The flow domain is shown in Fig. 1.

The Navier-Stokes and continuity equations, for the described flow, in non-dimensional form are,

$$\frac{\partial \vec{V}}{\partial t} + (\vec{V}\vec{\nabla})\vec{V} = -\vec{\nabla}p + \frac{1}{\mathrm{Re}}\nu\vec{\nabla}^2\vec{V} \qquad (1)$$

$$\vec{\nabla}\vec{V} = 0 \qquad (2)$$

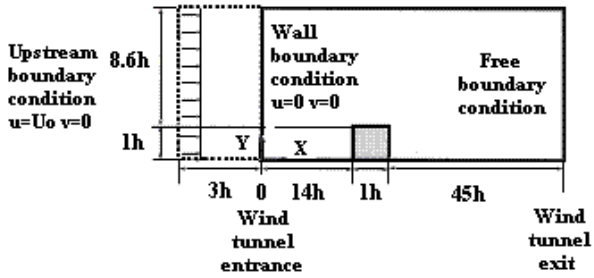

Figure 1. Computational domain of nominally two dimensional flow over a mounted obstacle.

The Reynolds number is calculated with respect to the height of the obstacle and the inlet free stream velocity and is equal to Re = 1304. The boundary conditions upstream of the entrance of the computational domain are a uniform free stream. The no-slip boundary conditions are imposed along the walls of the wind tunnel and the obstacle. The free boundary condition, is the outlet boundary which lets the fluid leave the computational domain freely without distortion, [5, 10]. The initial condition is given by solving the two-dimensional Navier-Stokes equations at t=0 and $(\mathrm{Re})_h$=1, [5].

2.1 Finite Element Formulation – Spatial and Time Advancements

To solve the governing equations (1) and (2), the finite element method has been used. The pressure was formulated by a linear basic function, while the

velocity by a quadric. The unknown velocities and pressure were expanded in Galerkin basic functions. Equations (1) and (2) were weighted integrally with the basic functions. Finally, applying the divergence theory, the following weight residuals were received,

$$R_c^i = \int_{\forall} \vec{\nabla}\vec{V}\psi^i d\forall \qquad (3)$$

$$R_M^i = \int_{\forall} [\frac{\partial \vec{V}}{\partial t} + \vec{V}\vec{\nabla}\vec{V} - \vec{\nabla}(-pI + \frac{1}{\mathrm{Re}}T)]\Phi^i d\forall \qquad (4)$$

Where $\vec{V}$ is the vector of velocity, I is the identity matrix, $T = \nabla\vec{V} + (\nabla\vec{V})^T$ is the stress tensor of the Newtonian fluid with $\nabla^2\vec{V} = \nabla T$, $d\forall$ is the infinitely small volume of calculating domain and Ψ^i, Φ^i are the linear and quadratic basic functions in equations (3) and (4) respectively.

The non linear system of equations (3) and (4) was solved numerically with the Newton-Raphson method. The flow domain was tessellated in 14645 finite elements with 59299 nodes and 133603 unknowns. The time-step was fixed at $\Delta t=0.01\ h/U_o$. At each space-point 15.000 instant samples were computed at a total time T=150. Each time-step needed three runs to converge. The biggest error of Newton-Raphson method was 10^{-6} for velocities and $5x10^{-4}$ for pressure calculations. Each run uses 2 CPU minutes.

3. Results and Discussion

3.1 Instantaneous and Time Mean-averaged Flow Values.

The separation and reattachment positions of the flow over a mounted-obstacle can be determined using three different methods according to Le et al [9]. Figures 2a,b show instantaneous fluctuations of separation and reattachment of the present work and the mean value of them, as well, while Fig. 2c shows a qualitative comparison of instantaneous fluctuation of reattachment of Le et al [9].

The mean separation position of the present work was at x_s = 3.52h and the mean reattachment point at x_R = 4.77h. Le at al [9] reported a x_R= 6.0h and Jovic and Driver [8] measured x_R=6.0h. Acharya et al. [2] measured $x_R = (6.3 \pm 0.9)h$ and calculated x_R = 7.5h with the linear κ-ε model and x_R = 6.9h with the standard. Hwang et al. [7] predicted a x_R=6.9h. Probably the differences are due to different flow configurations [9], and to different numerical methods, [2], [7]. The instantaneous profiles of the stream-wise velocity u^* are shown in Figs. 3a,b, 4a,b and 5a,b, at selected positions and times . The reversed flow at the separation zone, Fig.3b, on the obstacle's top, Figs 4a,b, and at the recirculation region, Fig.5a, are shown. It is also shown, Fig 5b, that the obstacle affects the flow far downstream of the reattachment position. Figures 6a to d show a qualitative comparison of the time mean-averaged stream-wise velocity profiles, predicted by DNS models, by Le et al. [9], ((a) and (c)), and the present work, ((b) and (d)).

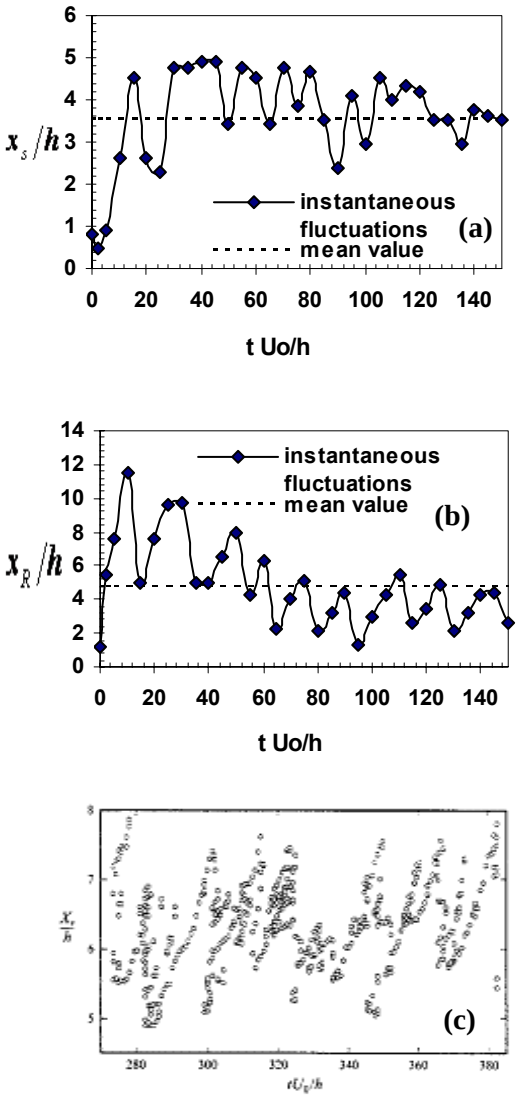

Figure 2 a,b,c. Instantaneous fluctuations and mean value of separation (a) and reattachment (b) of the present work. (c) Qualitative comparison of instantaneous fluctuations of reattachment of Le et al. [9].

The agreement looks rather good, but in the recirculation zone and near the wall, it seams that the present work gives better predictions than these of Le et al. [9]. Though both works have used a DNS model, it seams that the initial and upstream

boundary conditions, the numerical method of finite elements and the spatial and time advancements have improved the predicted values by calculating, besides the large, also the small vortices.

The fluctuations of instantaneous stream- wise and cross-stream velocities, u^* and v^*, are shown in Fig. 7 at x=5h downstream of the obstacle and at different height positions. It is shown that the time "lag" of the simulation time to allow the passage of initial transients, is $t=60h/U_o$. Although the fluctuations of the velocities look like showing a periodic pattern, there are visible turbulent characteristics. Those turbulent characteristics, which are the energy spectra of the kinetic energy of the component velocities u^* and v^* and the enstrophy spectrum, are shown, at x=5h and y=5h, in Figs. 8a,b,c. The calculations have been made with the commercial program Labview. The energy spectrum of u^* velocity has showed strong dependencies on both -5/3 and -3 power law of frequency. The enstrophy spectrum, shown in Fig. 8c, was calculated as one half of the square of vorticity and it shows an agreement with the -1 power law of frequency. The shown agreement in Figs. 8a,b,c, of the spectrum analysis with the theoretical results of a nominated two dimensional turbulence, has adequately given the accuracy to the numerical predictions.

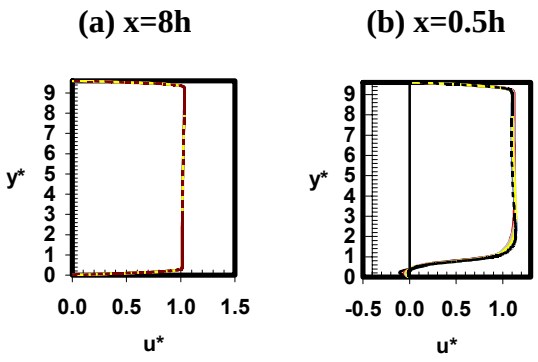

Figure 3 a, b. Calculated instantaneous velocity profiles of the streamwise velocity component upstream and at the separation region. Distances upwards from the obstacle.

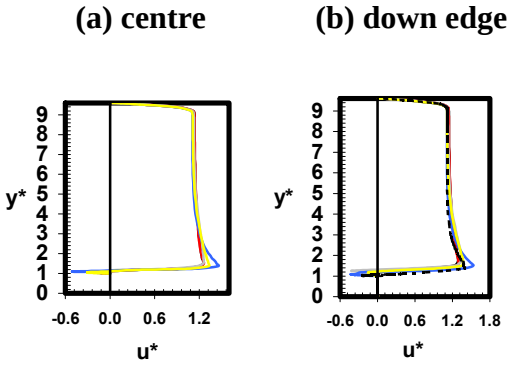

Figure 4 a,b,c Instantaneous velocity profiles on the top of the obstacle.

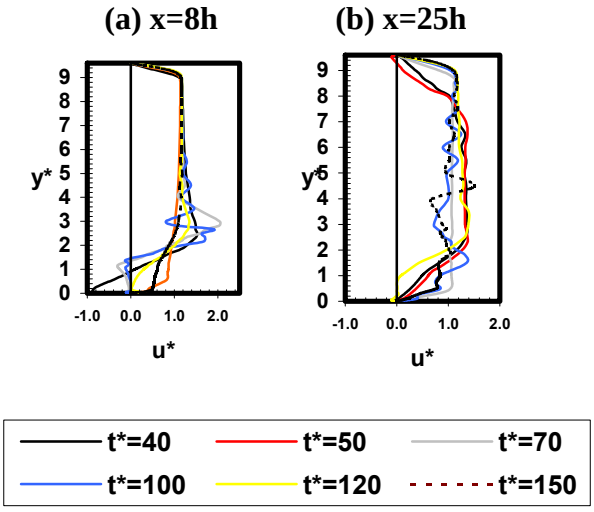

Figure 5 a,b. Instantaneous velocity profiles upstream and downstream of reattachment. Distances downstream of the obstacle.

3.2 Turbulent Intensities and Reynolds Stress

Figures 9a to d show turbulent intensity profiles calculated by using DNS models by Le et al. [9], (Figs. 9a,b) and present work, (Figs. 9c,d), in the neighborhood of reattachment. In Figs. 9a,b, the predicted profiles are compared to the experimental data, (dots), measured by Jovic and Driver [8]. Qualitative comparison of Le et al. simulated profiles to those of the present work shows that the peak of the calculated profiles of the present work are much bigger than those calculated by Le et al, in both turbulent intensities, stream-wise, (Figs. 9a,c) and cross-wise (Figs. 9b,d).

Figures 10a,b show Reynolds stress profiles downstream of a step, (Fig. 10a), and an obstacle, (Fig. 10b), calculated using DNS models, (Le et al. and present work). Near reattachment (x=4h) and downstream of it (x=6h), the peaks of the calculated profiles by Le et al. and the measured data by Jovic and Driver are only positive and much bigger than those in the present work. In the calculated profiles of the present work (Fig. 10b) there are major positive and minor negative peaks, while far downstream of reattachment (x=10h) there is only a negative peak. Further more, at x=19h, both simulated Reynolds stress profiles and those with experimental results look similar to a small positive peak.

3.3 Time Mean-Averaged Wall Shear Stress

The time mean-averaged wall stress for a two-dimensional flow has been calculated by the non-dimensional equation

$$\bar{\tau}_w^* = \frac{1}{(\mathrm{Re})_h}\left(\frac{\partial \bar{u}^*}{\partial \bar{y}^*} + \frac{\partial \bar{v}^*}{\partial \bar{x}^*}\right) \qquad (5)$$

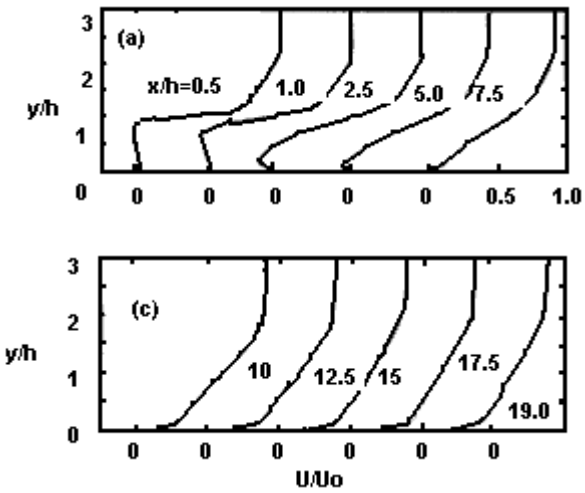

4. Conclusion

In this paper, the Navier-Stokes and continuity equations are numerically simulated to study a nominally two-dimensional flow over a rectangular wall-mounted obstacle where separation and reattachment occurs.

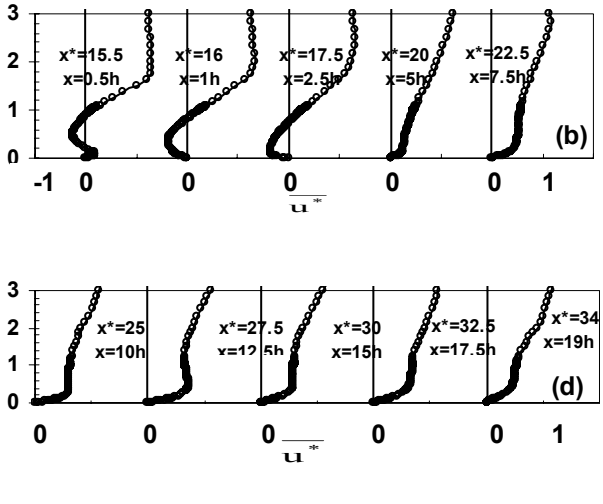

Figure 6 a to d Qualitative comparison of predicted mean stream-wise velocity profiles for different positions along x-axes with DNS model, (a) and (c) by Le et al. [9], (b) and (d), by the present work.

Figures 11a to e show the time mean-averaged wall stress distribution along the wall of the tunnel and along the obstacle's wall. The big drop in Fig. 11a is owed to initial conditions while those drops in Figs. 11b and c to the upper edge of the obstacle. The drop of Fig. 11d at $y^* = 1$ is owed to the down edge of the obstacle. The peaks of the wall stress distributions in Figs. 11d and e are owed to the recirculation region downstream of the obstacle.

Figures 12a, b show a qualitative comparison of the time mean-averaged skin friction coefficient predicted by DNS models by Le et al. [9], with experimental measurements by Jovik and Driver [8] and the present work. The skin friction coefficient is given by,

$$C_f = \frac{2\tau_w}{\rho U_o^2} = 2\bar{\tau}_w^* \qquad (6)$$

The similarity of the two figures is obvious, particularly in the recirculation area and the area just downstream of reattachment. Attention should be paid to the fact, that the value of the negative peak of the present work is almost equal to that of Le et al., while the first positive peak is bigger. Also the distribution line of the skin friction of the present work is not a smooth line as is the line of Le et al. These are due to the better predictions of velocity near the wall of the present work than the work of Le et al.

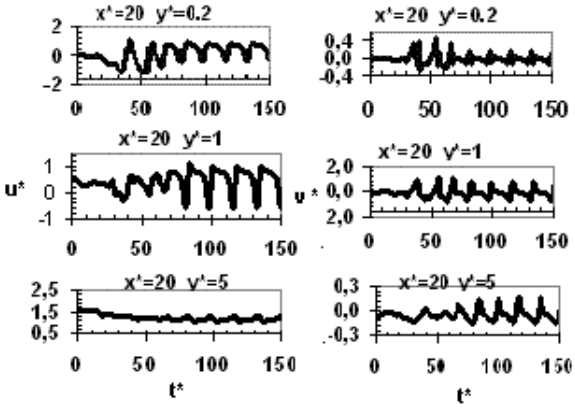

Figure 7. Fluctuations of instantaneous streamwise, u*, and cross-stream, v*, velocities at x=5h downstream of the obstacle at different height positions.

The Reynolds number was $(\mathrm{Re})_h = 1304$, based on the obstacle's height and inlet free stream velocity. The finite element method was used to solve the equations. A uniform free stream flow was imposed upon the entrance of the tunnel, the no-slip boundary conditions were applied along the walls of the tunnel and the obstacle and the free boundary condition was applied at the exit of the tunnel. As initial condition, a laminar flow solution at t=0 and $(\mathrm{Re})_h = 1$ was used.

The calculated reattachment position is the smallest measured or calculated one by others.

Probably, this is due to different flow configurations [8], [9], and to different numerical models used [2], [7]. The instantaneous velocity components have shown that the obstacle affected the flow far downstream of the reattachment position.

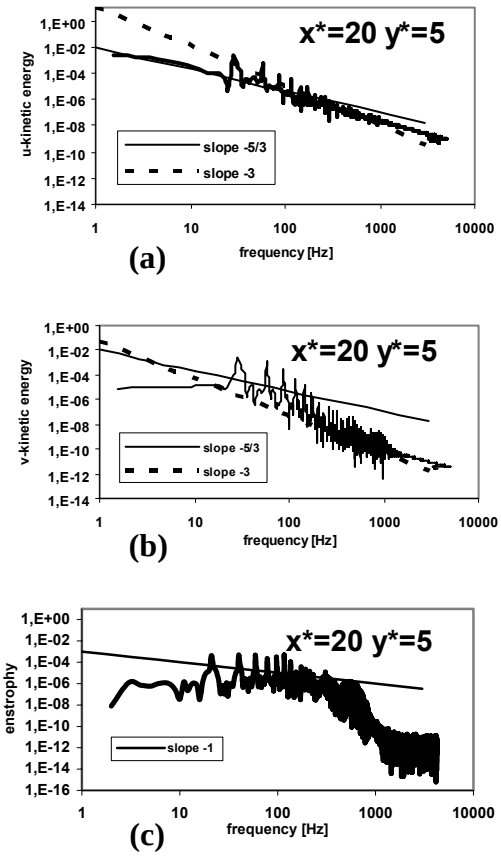

Figure 8 a,b,c. Energy spectra of the kinetic energy of the component velocities u* and v* and Enstrophy spectrum at x=5h, y=5h

Qualitative comparison of the time mean-averaged velocities with another DNS model shows rather good agreement, though the present work seams to give better predictions near the wall.

The fluctuations of instantaneous velocity components, the energy spectra of kinetic energy of them and the enstrophy spectrum show the turbulent characteristics of the flow. The dependencies of the -5/3 and -3 power law of frequency are rather strong while the enstrophy spectrum shows an agreement with the -1 power law of frequency. The above spectrum analysis is sufficient for the accuracy of the numerical predictions of the present work. Qualitative comparisons of the skin friction coefficient, using DNS models, show good agreement.

References

[1] Abdalla I.E. and Zhiyin Yang, Numerical Study of the Instability Mechanism in Transitional Separating-Reattaching Flow, *In. J. of Heat and Fluid Flow*, Vol. 25, 2004, pp. 593-605.

[2] Acharya S., Dutta S., Myrum T.A. and Baker R.S., Turbulent Flow past a Surface-Mounted Two-Dimensional Rib, *ASME J. Fluids Eng.*, Vol. 116, 1994, pp. 238-246.

[3] Acrivos A., Leal G.L., Snowden P.D. and Pan F., Further Experiments on Steady Separated Flows past Bluff Objects, *J.f Fluid Mechanics*, Vol. 34, 1968, pp. 25-48.

[4] Bergeles G.G. and Athanassiadis N., The Flow past a Surface-mounted Obstacle, *ASME,* J. *Fluid Eng*, Vol. 105, 1983, pp. 127-133.

[5] Fragos V.P., Psichoudaki S.P. and Malamataris N.A., Direct Computation of Turbulent Flow over a Surface Mounted Obstacle, *1st Int. Conf. "From Scientific Computing to Computational Engineering", Athens, Greece, 8-10 Sept,. 2004*.

[6] Friedrich R., Huttl T.J., Manhart M. and Wagner C., Direct Numerical Simulation of Incompressible Flows, *Computers and Fluids*, Vol. 30, 2001, pp.555-579.

[7] Hwang R.R., Chow Y.C. and Peng Y.F., Numerical Study of Turbulent Flow over Two-dimensional Surface Mounted Ribs in a Channel, *Int. J. Numer. Methods in Fluids*, Vol. 31, 1999, pp. 767-785.

[8] Jovic S. and Driver D.M., Backward-facing Step Measurement at Low Reynolds Number, $(Re)_h$=5000, *NASA Tech. Mem. 108807*, 1994.

[9] Le H., Moin P. and Kim J., Direct Numerical Simulation of Turbulent Flow over a Backward-facing Step, *J. Fluid Mech.*, Vol. 330, 1997, pp. 349-794.

[10] Malamataris N.A., *Computed-aided Analysis of Flows on Moving and Unbounded domains: Phase-change Fronts and Liquid Leveling*, Ph. D. Thesis, Univ. of Mich. Ann Arbor, 1991.

[11] Yaghoubi M. and Mahmoodi S., Experimental Study of Turbulent Separated and Reattached Flow over a Finite Blunt Plate, *Experimental Thermal and Fluid Science*, Vol. 29. 2004, pp. 105-112.

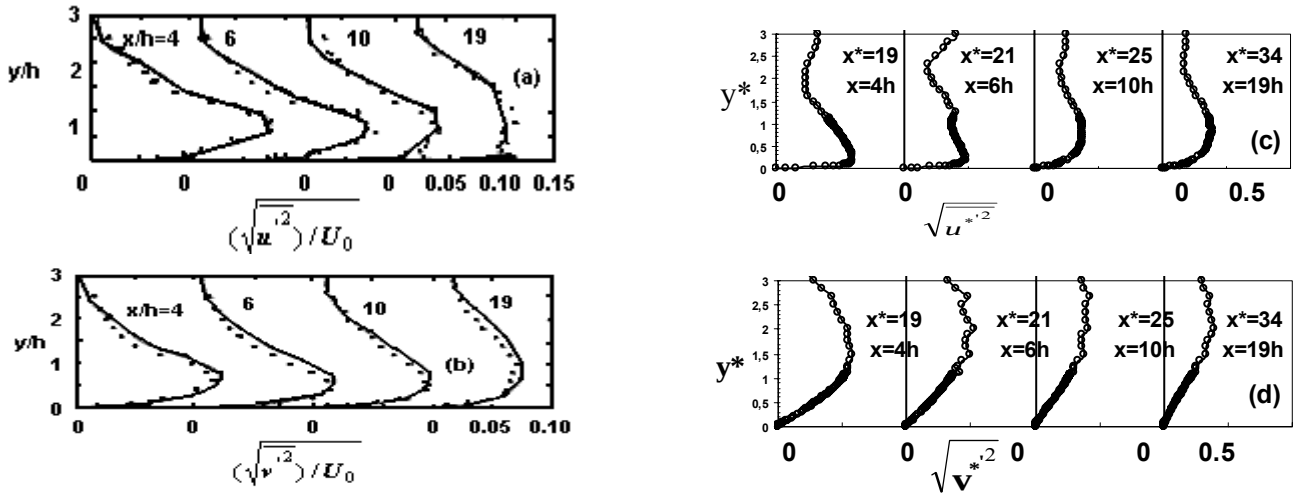

Figure 9 Qualitative comparison of predicted turbulent intensities, calculated by DNS models. (a) and (b) by Le et al. [9] (Dots: experimental data by Jovic and Driver [8]), (c) and (d) present work.

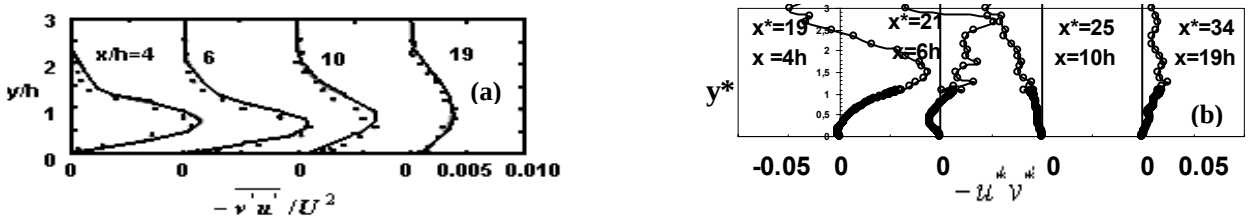

Figure 10 Qualitative comparison of predicted Reynolds stress with DNS models. (a) by Le et al. [9] (Dots: experimental data by Jovic and Driver [8]), (b) present work.

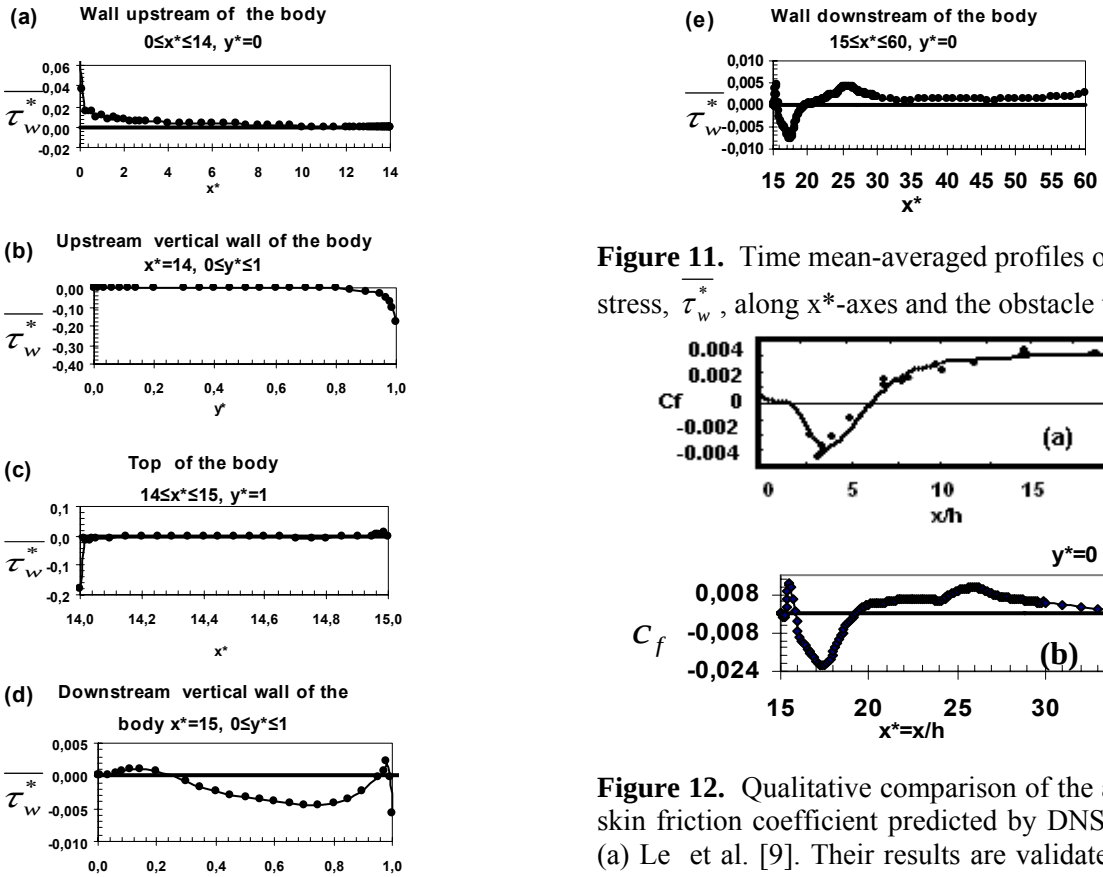

Figure 11. Time mean-averaged profiles of wall stress, $\overline{\tau_w^*}$, along x*-axes and the obstacle wall.

Figure 12. Qualitative comparison of the averaged skin friction coefficient predicted by DNS models. (a) Le et al. [9]. Their results are validated by the experimental data of Joves and Driver [8] (b) present work.